# PERFORMANCE EVALUATION OF ACCURATE TRIGGER GENERATION FOR VERTICAL HANDOVER


**Daniel Bültmann[1], Matthias Siebert[1], Matthias Lott[2]**

[1]Chair of Communication Networks, RWTH Aachen University, Aachen, Germany
[2]Siemens AG, Munich, Germany
[1]{dbn|mst}@comnets.rwth-aachen.de, [2]matthias.lott@siemens.com



***Abstract*—Cooperation amongst heterogeneous mobile radio systems will be an indispensable feature of 'beyond 3G'. One key mechanism thereby serving as enabling technique for system integration will be the Vertical HandOver (VHO) between different radio networks. Optimal handover control thereby is very important for which the present paper investigates a new algorithm for accurate VHO trigger generation. Taking the own position as input, mapping with location-based measurements from other stations is accomplished to decide for heterogeneous system coverage. Special interest thereby is laid on the fact that localization techniques inherently suffer from imprecision. Accurate trigger generation hence needs to overcome the impact of erroneous position information.**



***Index Terms*—System Integration, Vertical Handover, Kalman Filter, Coverage Detection**


## I. INTRODUCTION

FOLLOWING the evolution from 2G, over 3G and beyond, one will realize that the immanent drivers for this development are the users' basic needs for mobility and communication. The Always Best Connected [1] dogma will be of great importance for mobile users in future. It is not very likely that one single system will ever be able to deal with all demands of modern communication: Quality of Service requirements, security, maintainability, operation and deployment costs, spectrum scarceness, convenience, politics and health are only a few aspects that cannot all be optimized in parallel due to their partly contradictory objectives. Instead, the cooperation and bonding of dedicated technologies, each of which optimized for a specific task, entails a promising alternative.

Accordingly, many research projects of today such as [2] focus on aspects of system integration. However, to allow for smooth migration of services, the underlying techniques need to enclose some redundancy. The same holds, if a service started in one system, but for some reason cannot be completed there. In such a case, partly redundant network structures need to cushion imminent service interruption.

The main application scenario, to be investigated in many different specifications though, will be the connection of a Mobile Terminal (MT) to a system A (high coverage, moderate bit rate) with some intermediate handovers to another, vertical system B (low coverage, high bit rates) and probably back to system A again. The described case corresponds e.g. to a transition of a hotspot by a mobile device as shown in Figure 1. The corresponding handover between different systems A and B subsequently is referred to as *Vertical HandOver* (VHO).

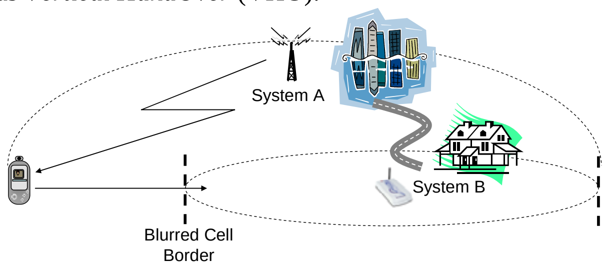


Figure 1: Exemplary scenario with two overlaying systems

VHO is one possible means to allow for (seamless) service continuity across network boundaries. Before sophisticated handover decisions may consider network switching, knowledge on alternatively available systems needs to be present first. This entails the initial detection of complementary systems. Especially, if mobility is involved, the accessible infrastructure changes quickly. This reduces the system integration aspect to the problem of coverage detection that needs to be solved prior to any further actions.

Coverage detection of a target system is conventionally realized by means of self-dependent scanning of the respective system. It was shown in [3] that this is not a preferable means to gather system information. Alternatively, one could imagine that existence and coverage of a potential target system is known due to measurements taken previously by other terminals. A concept that exploits foreign party based measurements, administers them in (long-term) databases and makes them available to other stations has been presented in [4]. Thus, considering these information only the own location is required to determine whether a VHO would be successful or not. However, the coverage area derived from the foreign party measurements does not comprise an accurate border, but can be better described by a widespread area with a blurred border, see Figure 1, owing to fading, interference and faulty positioning. Algorithms for VHO decision, considering all this input, need to find a way to compensate the blurring of the cell border as accurately as possible.

In [5] the authors presented the *Centre of Gravity* (CoG) algorithm that can be used for cell border detection based on foreign measurements associated with localization data. It was assumed that a mobile terminal's *exact* position is known when making VHO decisions. This paper investigates the impact of imprecise position information on the accuracy of the VHO decision.

The structure of the paper is as follows: Section II gives a short review of the CoG algorithm as proposed in [5]. Section III explains the error model that is used to emulate faulty positioning. In addition, movement prediction based on Kalman filtering is introduced. The simulation scenario and the performance of the CoG algorithm in conjunction with movement prediction are described in Sections IV and V. Finally, some concluding remarks in Section VI summarize achievements of this work. An appendix was added to explain important Kalman parameters and assumptions in more detail.

## II. The Centre of Gravity Algorithm for Coverage Detection

Accurate trigger generation based on foreign measurement reports needs to overcome the impact of localization errors.

The Centre of Gravity (CoG) algorithm was designed to compensate effects of 'misleading' measurements introduced to the database by erroneous positions. Thereby 'misleading' measurements are measurements that actually have been recorded inside the cell coverage. Due to positioning errors, associated coordinates reported along with the measurements indicate positions outside the actual coverage area. 'Correct' measurements suffer from the same positioning error but the reported position effectively is inside the cell coverage area. Both types are shown in Figure 2 as white ('misleading') and black ('correct') dots. The CoG algorithm exploits the fact that the density of 'misleading' measurements is lower than the density of 'correct' measurements.

Figure 2 illustrates the algorithm's outcome when a mobile terminal approaches the cell border. The algorithm calculates the distance from the mobile terminal to the CoG of all measurements within its vicinity (defined by the circular Decision Area (DA) with radius $R_{DA}$). The distance reported initially (1) is the radius of the DA itself. This is the case, as soon as the outer bound of the DA matches the position of the first single 'misleading' measurement report. Moving towards the cell border firstly decreases the distance to the CoG (2). When the DA further enters cell coverage (3) it includes 'correct' reports. Since these have a much higher density, the distance is likely to increase again. Finally, after the mobile terminal (and the DA) have passed by the actual cell border (4), the distance drops below a threshold that can be chosen for trigger generation.

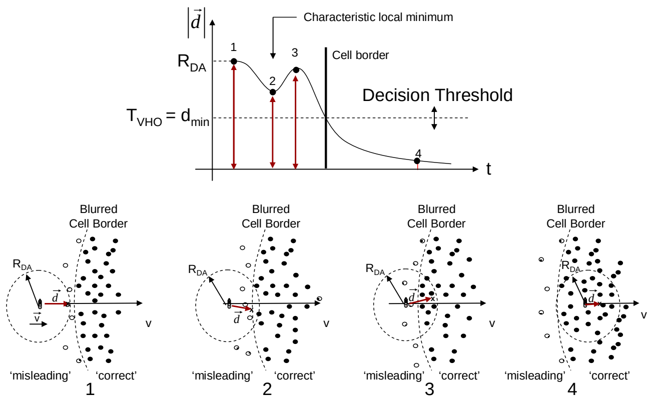


Figure 2: Centre of Gravity Algorithm [5]

So far, noisy positioning was assumed for measurements in the data base only, while the position of the terminal used as input for CoG requests inherently was assumed to be exact. In reality, this is not the case. Hence, this paper concentrates on the impact of imprecise terminal localization when performing VHO decisions with the CoG algorithm.

## III. Localization Error and Movement Prediction

This section introduces the localization error model used to emulate faulty positioning within the simulations of Section V. Basically, an augmented two-dimensional Gaussian distribution is applied. The second part of this section gives a description of the movement prediction that is introduced to overcome the influence of imprecise localization.

### A. Localization Error Model

Localization errors are modeled applying a two-dimensional Gaussian distribution for the position deviation with a cut-off at the maximum error of $r_{\max}$. It is assumed that unreasonable high positioning errors beyond $r_{\max}$ can be filtered out beforehand, e.g. by higher layer detection.

Furthermore, it is assumed that there is no correlation between the x and y coordinates ($\sigma'_{xy} = \sigma'_{yx} = 0$) and the variance both for x and y coordinates is the same ($\sigma'^2_{xx} = \sigma'^2_{yy} = \sigma'^2$). Using polar coordinates the Probability Density Function (PDF) for this distribution may be written as:

$$p(r) = \begin{cases} C + \dfrac{1}{2\pi\sigma'^2} e^{-\frac{r^2}{2\sigma'^2}} & \text{for } -r_{\max} \le r \le r_{\max} \\ 0 & \text{otherwise} \end{cases} \tag{1}$$

The cut-off at $\pm r_{\max}$ shifts the PDF by C. Using

$$\int_0^{2\pi}\int_0^{r_{\max}} p(r)\cdot r\cdot dr\cdot d\phi = 1 \text{ yields to } C = \frac{1}{\pi r^2_{\max}} e^{-\frac{r^2_{\max}}{2\sigma'^2}}. \tag{2}$$

The variance of this augmented Gaussian distribution may be calculated by solving

$$\sigma_{xx}^2 = \int_0^{2\pi} \int_0^{r_{\max}} p(r) \cdot r^3 \cos^2(\phi) \cdot dr \cdot d\phi \tag{3}$$

and

$$\sigma_{yy}^2 = \int_0^{2\pi} \int_0^{r_{\max}} p(r) \cdot r^3 \sin^2(\phi) \cdot dr \cdot d\phi. \tag{4}$$

The variance of position measurements may be expressed by the cut-off $r_{\max}$ and the variance of the original distribution $\sigma'$:

$$\sigma_R^2 = \sigma_{xx}^2 = \sigma_{yy}^2 = \sigma'^2 \left(1 - \left(1 + \frac{r^2_{\max}}{4\sigma'^2}\right) e^{-\frac{r^2_{\max}}{2\sigma'^2}}\right). \tag{5}$$

Knowledge on the statistical properties of the measurement error is needed for successful application of the Kalman Filter for movement prediction introduced in the following section.

### B. *Movement Prediction using Kalman Filter*

The Kalman Filter addresses the general problem of trying to estimate the state vector $x_k \in \Re^n$ of a discrete-time controlled process that is governed by the linear stochastic difference equation [6]:

$$x_k = \mathbf{A} x_{k-1} + \mathbf{B} u_k + w_k \tag{6}$$

Estimation of the process state is done by taking measurements which are given by:

$$z_k = \mathbf{H} \cdot x_k + v_k \tag{7}$$

The random variables $w_k$ and $v_k$ represent the process and measurement noise. They are assumed to be independent, white and with normal probability distributions. The process noise covariance matrix is denoted by $\mathbf{Q}$ and measurement covariance matrix by $\mathbf{R}$.

Figure 3 shows the general structure of the Kalman Filter. On top, a block diagram of equations (6) and (7) is shown. This is the discrete-time representation of the system with unknown state vector $x_k$.

The bottom part shows the Kalman Filter that is used to estimate the process state vector $x_k$. A replication of the original system is used to derive the estimate state vector $\hat{x}_k$. Each time-step a *time update* is performed that calculates a prediction of the system output. This is done by

$$\hat{x}_k^- = \mathbf{A} \hat{x}_{k-1} + \mathbf{B} u_{k-1} \tag{8}$$

Please note that the minus sign indicates that this value is an a priori value which is predicted and has not yet taken into account the newly arriving measurement. The time update is finished by calculating the a priori error covariance matrix $\mathbf{P}_k^- = \mathbf{A}\mathbf{P}_{k-1}\mathbf{A}^T + \mathbf{Q}$. Predicted values for the state vector $\hat{x}_k^-$ and the error covariance matrix $\mathbf{P}_k^-$ are used during

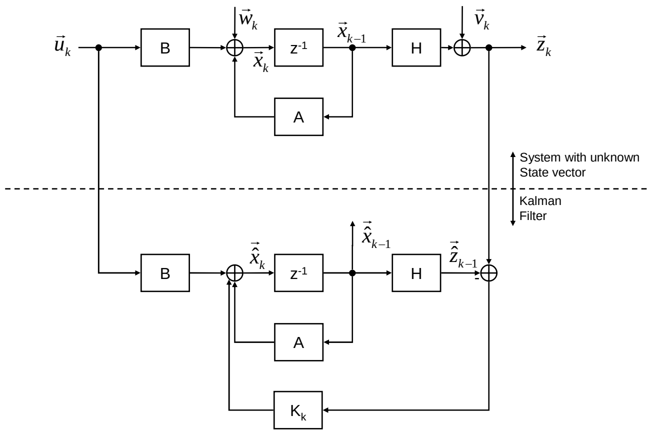


Figure 3: General Structure of the Kalman Filter

the *measurement update* step to correct the system. The Kalman Gain $\mathbf{K_k}$ is adjusted in a way that the a posteriori error covariance is minimized [6]. It gives a measure on how much the prediction $\hat{x}_k^-$ and on how much the measurement $z_k$ is trusted. The Kalman gain is given by:

$$\mathbf{K}_k = \mathbf{P}_k^- \mathbf{H}^T (\mathbf{H}\mathbf{P}_k^- \mathbf{H}^T + \mathbf{R})^{-1}, \tag{9}$$

the state vector estimation with current measurement $z_k$ by

$$\hat{x}_k = \hat{x}_k^- + \mathbf{K}_k (z_k - \mathbf{H}\hat{x}_k^-), \tag{10}$$

and the error covariance matrix update by

$$\mathbf{P}_k = (\mathbf{I} - \mathbf{K}_k \mathbf{H}) \mathbf{P}_k^-. \tag{11}$$

The appendix lists detailed information on the actual model parameters used in the filter implementation throughout all the simulations.

## IV. Simulation Scenario

There are two different scenarios evaluated within this paper. The first is used to evaluate the performance of movement prediction for different localization precisions. Analysis of the VHO trigger accuracy using the CoG algorithm with imprecise positioning is done with the second scenario.

### A. *Movement Prediction Scenario*

The performance of position estimation by Kalman filtering, described in Section III is evaluated by estimating the trajectory of a pedestrian mobile user moving according to a random mobility model illustrated by Figure 4. Mobile terminals move straightforward with a constant velocity $\vec{v}$ for a randomly chosen distance $d_1$. Then the direction is altered by a randomly chosen angle between $\pm\varphi$ degree (chosen here to 5 degree) and a new distance ($d_2$) is randomly drawn. This is used as input data to the Kalman filter. The performance is analyzed by evaluating the statistical properties of the estimation error.

underlying Gaussian distribution was set to 10m, too.

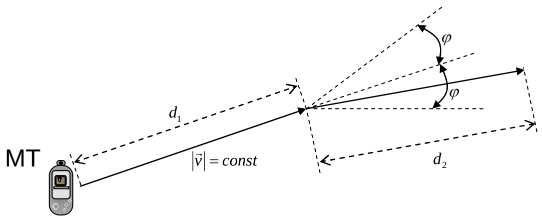


Figure 4: Random Mobility Model

### B. Centre of Gravity Scenario

The CoG algorithm's performance using erroneous localization is evaluated in the scenario shown in Figure 5. A mobile terminal (MT) approaches the coverage area of a WLAN (IEEE 802.11a) Access Point (AP).

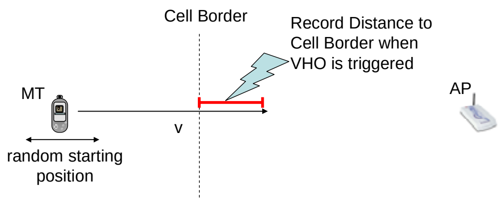


Figure 5: Simulation Scenario

The starting point is chosen randomly. The mobile terminal moves with constant velocity of v = 5 km/h. Every 200ms, localization is performed and the CoG algorithm is used to make a handover decision. The decision area radius was chosen to 5m. If the algorithm triggers a handover to the destination system the distance of the mobile terminal to the cell border is recorded. The probability distribution of this distance is derived from consecutive simulation runs.

The cell border is determined by the minimum sensitivity required by IEEE 802.11a for BPSK1/2 of -82dBm. The distance is derived from a single slope propagation model with path loss coefficient of $\gamma = 2.4$ given by

$$P_r(d) = \begin{cases} P_s \cdot g_s g_r \left(\dfrac{\lambda}{4\pi d_0}\right)^2 & d \le d_0 \\ & \text{for fixed } d_0 = 1m \,. \\ P_s \cdot g_s g_r \left(\dfrac{\lambda}{4\pi d_0}\right)^2 \left(\dfrac{d_0}{d}\right)^{\gamma} & d > d_0 \end{cases} \qquad (12)$$

Thereby $P_S$ and $P_R$ denote the transmission and reception power $g_S$ and $g_R$ the antenna gain at sender and receiver and $d$ denotes the distance between sender and receiver. Assuming no antenna gain and using 100mW transmission power results to a cell radius of 191m (f=5.5GHz). Positioning errors where modeled according to Section III with different parameters for maximum error and variance. It is assumed that the measurements recorded in the database beforehand were associated with positions that suffer from erroneous localization where the maximum error was set to 10m and the standard deviation $\sigma'$ of the underlying Gaussian distribution was set to 10m, too.

## V. Performance Evaluation

### A. Kalman Filter Performance

Figure 6 shows the trajectory estimation performed by our movement prediction. Every 200ms the mobile terminal's position is measured and the time and measurement update steps (equation (9)-(11)) are performed. The localization error model was set to a maximal error of 10m and a standard deviation of 10m.

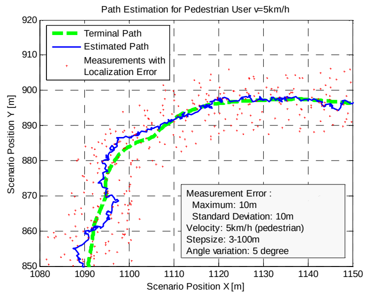


Figure 6: Sample trajectory estimation

The dashed line shows the terminal's trajectory generated by the mobility model, the solid line shows the estimated trajectory and the single dots show the measured positions including the associated positioning error. It can be seen that measurements are located within 10 meters around the trajectory. The estimated path is very close to the actual trajectory. These simulations were repeated for different measurement error parameters. The estimation errors are normally distributed with zero mean. Table 1 shows the standard deviation along with the 95% circular error margin. The absolute estimation error is below that margin for 95% of all estimates.

It can be seen that there is a significant precision improvement when using movement prediction. Thereby the improved precision is at the expense of increased measurement frequency.

Table 1: Estimation Error Variance for different Error model parameters

| Localization Error Model | | Estimation Error | |
|---|---|---|---|
| Maximum Error [m] | Standard Deviation $\sigma'$ [m] | 95% Circ. Error Margin [m] | Standard Deviation [m] |
| 10m | 10m | 3.25m | 1.33m |
| 50m | 50m | 11m | 4.46m |
| 150m | 150m | 24.8m | 10.20m |
| 200m | 200m | 30.8m | 12.65m |

This makes it especially attractive for solely network based localization methods which usually suffer from lower precision compared to, e.g. terminal on-board GPS, but that can be conducted much more often. Summarizing this Section, Kalman filtering is applied to significantly improve the position estimation of a terminal moving towards the coverage area of a radio system. Since the own position is used as input for CoG database queries, it is important to be as precise as possible. However, the own position is only one out of three aspects that affect CoG reliability. The following section addresses all three aspects and provides respective CoG performances.

### *B. Centre of Gravity Algorithm Performance*

The coverage detection accuracy of the CoG algorithm basically depends on three parameters, i.e. Top 1) the number of measurements within the database, Top 2) the chosen Decision Threshold (see Figure 2), and Top 3) the positioning error that is made when locating the respective mobile terminal.

Top 1): Figure 7 shows the impact of different measurement densities on the accuracy of the handover decision. It shows the cumulative distribution function of the distance from mobile terminal to cell border when handover is triggered. The CoG algorithm threshold was set to 0.25m and there is no positioning error for the moving terminal.

However, database entries ('misleading' and 'correct' reports, see Figure 2), with which the moving terminal's position is compared, certainly suffer from erroneous localization (variance 10m and maximal error 10m). It can be seen that with increasing measurements within the decision area the CoG detection of the actual coverage border improves. There are up to 20% of decisions that are made too early, this would result in ping-pong handover.

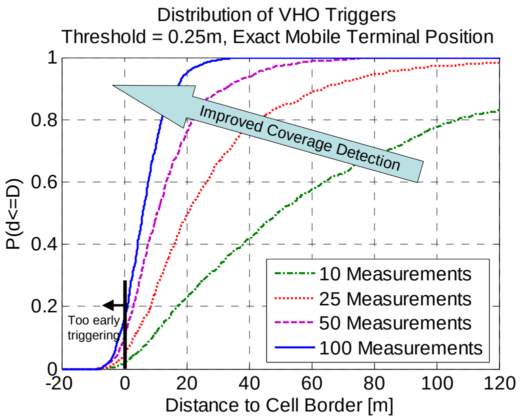


Figure 7: VHO precision for different measurement densities

However, since these handover triggers have to be signaled to the mobile terminal, it could be a benefit to be informed prior to actually reaching the cell.

Top 2) Figure 8 shows the impact of different threshold values on the trigger distribution. It can be seen that with increasing threshold more and more handovers are triggered too early. With low thresholds it is possible that triggers are generated very late. This due to the fact that within the cell the measurement density is not constant, therefore the distance to the CoG has a certain jitter. If the threshold drops down and is within the same order as the jitter it is possible that the threshold is passed very late.

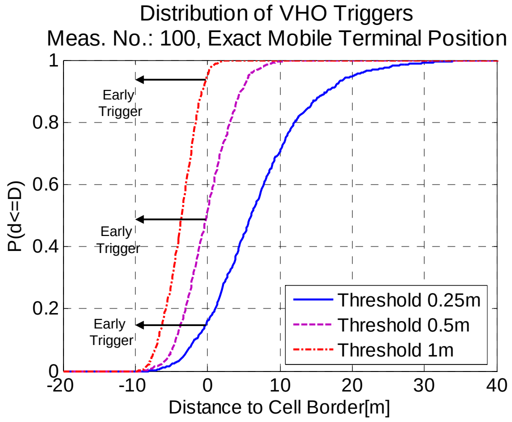


Figure 8: VHO trigger Distribution for different CoG thresholds

Top 3): Figure 9, finally shows the impact of localization errors for the moving mobile terminal. The values shown in Table 1 were used to set the maximal error and standard deviation of the error model described in Section III. The maximal error was set a little higher than the 95% border to give account for the truncation. Gains due to Kalman movement prediction were taken into account by an accordingly decreased positioning error.

The rightmost curve represents the case where the approaching mobile terminal is exactly located. Clearly, precision decreases with increasing positioning error. It is interesting to see that even the for the case with maximal error of 12m, which corresponds to the localization error of 50m in Table 1, reasonable good performance is achieved. For larger positioning errors more and more handovers are triggered before the actual cell border is reached. However, movement prediction not only supplies the current position but the velocity and acceleration vector, too. This could be exploited to overcome these early VHO triggers. Very late handover decisions beyond 15m inside the coverage area do

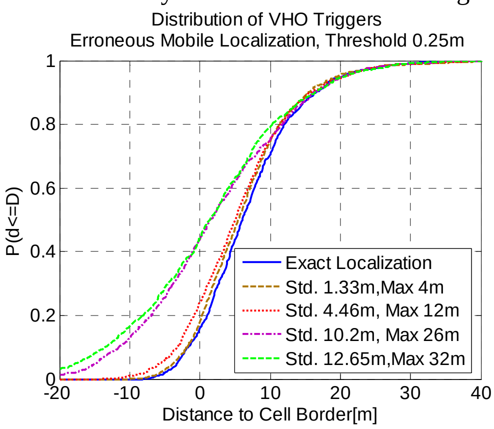


Figure 9: VHO trigger distribution for different localization errors

not depend anymore on the localization error. The farer mobile terminals are within the coverage area the higher the probability that the reported imprecise location is well within the coverage area, too. The handover probability therefore only depends on the measurement distribution (investigated in Top 1) within the cell.

## VI. Conclusions

A method for vertical handover trigger generation based on the CoG algorithm [5] was presented and evaluated. It specifically deals with imprecise localization impacts. It has been shown that this imprecision can be overcome by using movement prediction to improve the performance of respective localization methods, thereby trading frequency of measurements for localization accuracy. The impact of erroneous positions on the vertical handover decision was evaluated and it was shown that improvements for accurate trigger generation are possible. Next steps will be to evaluate further possibilities imposed by movement prediction. The Kalman filter also supplies the velocity and acceleration vector, which can be used to further improve VHO decisions by adjusting the time when a VHO is signaled to the mobile terminal. By now, only the absolute value of the distance vector from the mobile terminal to centre of gravity is evaluated. Both, velocity vector and distance vector, can be used to detect mobile terminals moving parallel to cell borders to decrease the amount of ping-pong handovers.

## Appendix

This section lists the detailed parameters for Kalman filtering as described in Section III mainly taken from [7] and [8]. All values are given for the one-dimensional case. The two-dimensional equation can be derived by calculating the Kronecker product with the 2x2 identity matrix, e.g. $\mathbf{A}_{2-\dim} = \mathbf{I}_2 \otimes \mathbf{A}$. The estimated state vector within the simulation encompasses the mobile's position, velocity and acceleration $\hat{x} = (\hat{x}, \hat{v}_x, \hat{a}_x)$. There are no external inputs to the system: $\mathbf{B} = 0$. Mobility is modeled by the process noise. All values listed are based on an acceleration model, where the acceleration is correlated in time according to the correlation function with time constant $\alpha$ and acceleration variance $\sigma_m^2$: $r_a(\tau) = E\{a(t)a(t+\tau)\} = \sigma_m^2 e^{-\alpha|\tau|}$. The corresponding differential equation for a is $\dot{a} = -\alpha \cdot a + \sqrt{2\sigma_m \alpha} \cdot w(t)$. This yields to the continuous model for this case

$$\dot{x} = \underbrace{\begin{pmatrix} 0 & 1 & 0 \\ 0 & 0 & 1 \\ 0 & 0 & -\alpha \end{pmatrix}}_{\mathbf{F}} x + \underbrace{\begin{pmatrix} 0 \\ 0 \\ \sqrt{2\sigma^2\alpha} \end{pmatrix}}_{\mathbf{G}} w(t) \tag{13}$$

The time discrete system matrix $\mathbf{A}$ is given by (20). Observations are only made on the position information of the estimated state vector: $\mathbf{H} = \begin{pmatrix} 1 & 0 & 0 \end{pmatrix}$. The covariance matrix of the system noise $\mathbf{Q}$ that describes random accelerations made by the mobile terminal is given by [8][9]

$$\mathbf{Q} = 2\alpha\sigma_m^2 \begin{pmatrix} q_{11} & q_{12} & q_{13} \\ q_{12} & q_{22} & q_{23} \\ q_{13} & q_{23} & q_{33} \end{pmatrix} \tag{14}$$

$$q_{11} = \frac{1}{2\alpha^5}\left(1 + 2\alpha T - e^{-2\alpha T} - 2\alpha^2 T^2 + \frac{2}{3}\alpha^3 T^3 - 4\alpha T e^{-\alpha T}\right) \tag{15}$$

$$q_{12} = \frac{1}{2\alpha^4}\left(1 - 2\alpha T + e^{-2\alpha T} + \alpha^2 T^2 - 2e^{-\alpha T} + 2\alpha T e^{-\alpha T}\right) \tag{16}$$

$$q_{13} = \frac{1}{2\alpha^3}\left(1 - e^{-2\alpha T} - 2\alpha T e^{-\alpha T}\right) \tag{17}$$

$$q_{22} = \frac{1}{2\alpha^3}\left(4e^{-\alpha T} - 3 - e^{-2\alpha T} + 2\alpha T\right) \tag{18}$$

$$q_{23} = \frac{1}{2\alpha^2}\left(e^{-2\alpha T} - 2e^{-\alpha T} + 1\right),\ q_{33} = \frac{1}{2\alpha}\left(1 - e^{-2\alpha T}\right) \tag{19}$$

$$\mathbf{A} = \mathbf{L}^{-1}\left\{(s\mathbf{I} - \mathbf{F})^{-1}\right\} = \begin{pmatrix} 1 & T & \frac{1}{\alpha^2}\left(\alpha T - 1 + e^{-\alpha T}\right) \\ 0 & 1 & \frac{1}{\alpha}\left(1 - e^{-\alpha T}\right) \\ 0 & 0 & e^{-\alpha T} \end{pmatrix}. \tag{20}$$

The error covariance matrix is initialized by

$$\mathbf{P}_0 = \begin{pmatrix} \sigma_R^2 & \frac{\sigma_R^2}{T} & 0 \\ \frac{\sigma_R^2}{T} & p_{22} & \frac{\sigma_m^2}{\alpha^2 T}\left(e^{-\alpha T} + \alpha T - 1\right) \\ 0 & \frac{\sigma_m^2}{\alpha^2 T}\left(e^{-\alpha T} + \alpha T - 1\right) & \sigma_m^2 \end{pmatrix} \tag{21}$$

With

$$p_{22} = 2\frac{\sigma_R^2}{T^2} + \frac{\sigma_m^2}{\alpha^2 T}\left(2 - \alpha^2 T^2 + \frac{2}{3}\alpha^3 T^3 - 2e^{-\alpha T} - 2\alpha T e^{-\alpha T}\right) \tag{22}$$

The state vector is initialized by the mean of the first two measurements. The initial velocity is the difference of both measurements divided by the sampling period.

## References


[1] M. O'Droma et al., "Always Best Connected" Enabled 4G Wireless World," Proc. 12th IST Summit on Mobile and Wireless Commun., Aveiro, Portugal, June 2003, pp. 710-16

[2] IST-2001-38835 ANWIRE, D1.5.1, “Integrated System and Service Architecture”, June 2003

[3] Schinnenburg et al. “Enhanced Measurement Procedures for Vertical Handover in Heterogeneous Wireless Systems”, 14th International Symposium on Personal, Indoor and Mobile Radio Communications (PIMRC), p.p. 166-171, Beijing, China, Sept. 2003

[4] Siebert, et al., “Hybrid Information System”, Proceedings of IEEE Semiannual Vehicular Technology Conference (VTC2004-Spring), Milan, Italy, May 2004

[5] Siebert, Bültmann, Lott, “Inter-System Handover and Coverage Detection for 3G/WLAN Cooperation”, In Proceedings of 11th European Wireless Conference 2005, p.p. 328-336, Nicosia, Cyprus, 04/2005

[6] G. Welch and G. Bishop, “An Introduction to the Kalman Filter”, www.cs.unc.edu/~welch/kalman/kalmanIntro.html, April 2004

[7] B. L. Mark, Z. R. Zaidi, “Robust Mobility Tracking for Cellular Networks”, IEEE International Conference on Communications, p.p. 445-449, New York May 2002

[8] T. Liu, P. Bahl and I. Chlamtac, “Mobility Modeling, Location Tracking, and Trajectory Prediction in Wireless ATM Networks”, IEEE Journal on Selected Areas in Communications Vol. 16 Issue 6, p.p. 922-936, Aug. 1998

[9] R.G. Brown, “Introduction to Random Signal Analysis and Kalman Filtering”, John Wiley & Sons, 1983